Research Article | Vol. 34, No. 16 / 10 Aug 2026 / *Optics Express* 28972

Optics EXPRESS

Rapid fabrication of height-tunable high-aspect-ratio voxels by tailored Bessel beams

TONGYAN LIU,[1] YUE YANG,[1] RUIQI WANG,[1] FRANÇOIS COURVOISIER,[2] MINGLIE HU,[1] AND CHEN XIE[1,*]

[1] *Ultrafast Laser Laboratory, Key Laboratory of Opto-Electronic Information Technology, Ministry of Education, School of Precision Instruments and Opto-Electronics Engineering, Tianjin University, Tianjin 300072, China*

[2] *Université Marie et Louis Pasteur, CNRS, Institut FEMTO-ST, F-25000 Besançon, France*

[*] *xie_chen@tju.edu.cn*

Abstract: We present a fast method to produce height-controllable high-aspect-ratio (HAR) voxels in the two-photon polymerization process. By loading complex-amplitude encoded holograms onto a phase-only spatial light modulator (SLM), precise control over the axial intensity profile of a Bessel beam is achieved, enabling the fabrication of height-tunable HAR voxels in a single exposure without mechanical axial motion. The voxel height can be adjusted independently and continuously over a range of 15 µm while maintaining the constant lateral size of 1.3 µm simply by switching tailored Bessel beam holograms. As demonstrated, microneedle arrays and hollow circular and polygonal microtubes with graded heights were fabricated.

1. Introduction

Two-photon polymerization (TPP) has been widely used in the fabrication of microstructures across various fields including biomedicine [1], micro/nano-optics [2,3], and microfluidics [4] for its true three-dimensional processing ability and sub-diffraction-limited processing precision. Improving the processing throughput has been deemed as the key factor for the industrialization of TPP [5]. Various high-speed fabrication strategies have been proposed to greatly boost the fabrication efficiency compared with the 3D point-by-point laser direct writing (LDW). In the parallel processing schemes, multi-foci patterned light fields are generated via the diffraction devices like digital micromirror device (DMD) [6] or LCoS-SLM [7], allowing even more than one thousand voxels to be generated simultaneously. Further fine motion control over this, introducing high-speed scanning devices like galvanometric mirrors enhance the system throughput to 10^8 voxel/s [8–10], enabling rapid fabrication of large-area structures. Another methodology involves laser beam shaping techniques, by utilizing LCoS-SLM, an incident beam—typically the Gaussian beam—can be transformed into a special beam with a prescribed intensity profile, such as the Bessel beam [11,12], or abruptly autofocusing beam [13]. By tuning the beam parameters, a corresponding three-dimensional microstructure can be rapidly created via a single exposure [14,15]. Through this approach, researchers have achieved rapid fabrication of functional surface [16], microtubes [17–19], and chiral structures [20].

Among these applications, high-aspect-ratio (HAR) microstructures have emerged as a particularly important class, for their wide applications such as microneedle arrays for drug delivering [21]. Various methods for generating HAR microstructures via two-photon polymerization have been reported, including rapid axial scanning [22–24], scanning between pre-existing micro-pillars with a low-power laser [25], and single exposure using long depth focal beam like Bessel beams [26] or axilens beams [27]. Among the above schemes, one-step single exposure methods enable fast fabrication due to the inherent HAR voxels induced by the structured long

#599852 https://doi.org/10.1364/OE.599852
Journal © 2026 Received 24 Mar 2026; revised 12 Jun 2026; accepted 12 Jul 2026; published 28 Jul 2026

Optics EXPRESS

focal beams. However, independent control over the voxel height remains a challenge. Commonly employed strategies rely primarily on mechanically adjusting the immersed beam depth into the photoresist using precision translation stages [28], which introduces inherent mechanical latency and thus limits the fabrication throughput. Varying the total exposed power of the input beam may offer an alternative, but it leads to coupled changes in different voxel features [26,29]. Pan et al. demonstrated the rapid fabrication of HAR microstructures using specially-optimized beams with long focal depth [28]. However, adjusting the beam length by tuning the focusing properties of the axilens still introduces an undesired axial displacement of the beam.

Here, we present a pure holography-based method for generating height-tunable HAR voxels by precisely tailoring the axial intensity profile of femtosecond Bessel beams. We engineer the longitudinal spatial spectrum to create Bessel beams with a flat-top longitudinal profile having a controllable length. By simply switching holograms in the one-step exposure procedure, the HAR voxel height can be adjusted continuously over 15 µm while maintaining the lateral dimension and without any axial mechanical motion in the fabrication. Compared with existing strategies in which height control inevitably couples with lateral expansion or time-consuming stage motion is involved, our straightforward approach offers a non-mechanical, high-speed alternative that ensures independent feature control and enhanced processing stability. As a demonstration, microtubes and polygonal microstructure arrays fabricated with this HAR voxel confirms the suitability of this technique for high-precision rapid fabrication of complex three-dimensional HAR micro/nano-structures.

2. Method and principle

To generate length-tunable Bessel beams for HAR voxels fabrication, we employed our previous method for engineering the on-axis intensity profiles of Bessel beams [30]. Under the paraxial and scalar approximations, the radially symmetric optical field $E(r, z = 0)$ in the initial plane can be expressed as:

$$E(r, z = 0) = \frac{1}{2\pi} \int_0^\infty S(k_r, z = 0) J_0(k_r r) k_r dk_r \tag{1}$$

where r is the radial coordinate, z is the propagation distance, k_r represents the radial spatial frequency, S is the amplitude of the spatial spectrum, and J_0 is the first kind zero-order Bessel function. For a given on-axis intensity distribution $I(z) \equiv |U(r = 0, z)|$, the spatial spectrum S can be expressed as:

$$S\left(\sqrt{k_0^2 - k_z^2}, z = 0\right) = \frac{1}{k_z} \int_0^\infty \sqrt{I(z)} \exp[i(k_{z0} - k_z)z] dz \tag{2}$$

Here, k_{z0} and k_z respectively represent the wave-vector and the longitudinal spatial frequency of the beam. By resolving Eq. (2), the spectrum S in the input plane for any prescribed axial intensity profile $I(z)$ can be derived. Furthermore, the target complex optical field distribution $E_d(x, y)$ can be calculated by substituting S into Eq. (1). Based on Eq. (2), we can further generate Bessel beams with an engineered on-axis intensity profile. Details on tailoring the corresponding spectrum are well explained in our previous work [30].

The experimental setup is illustrated in Fig. 1(a). The incident femtosecond laser beam (Pharos, Light Conversion; central wavelength: 1030 nm; pulse duration: ∼270 fs; repetition rate: 100 kHz) was frequency-doubled by a BBO crystal and the second-harmonic wave at 515 nm was reflected by a phase-only spatial light modulator (SLM, Holoeye PLUTO, 1920 × 1080 pixels, pixel pitch: 8 µm, 60 Hz refresh rate). A complex amplitude modulation phase mask, as shown in Fig. 1(b), was loaded onto the SLM to transform the incident Gaussian beam into the tailored Bessel beam. The resulting modulated -1^{st} order beam was then demagnified through a 2f-2f confocal telescope system with a total demagnification of ∼1/278 (lens, f = 1 m;

Optics EXPRESS

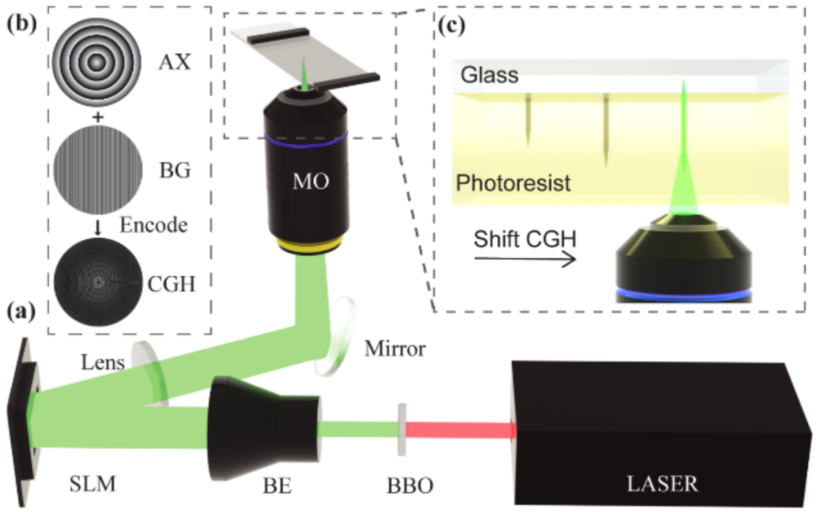

Fig. 1. (a) Schematic of the femtosecond laser fabrication system. SLM: spatial light modulator; MO: microscope objective. BE, beam expander. (b) Computer-generated hologram (CGH) for generating Bessel beam with tailored axial intensity. AX: axicon phase mask. BG: blaze grating. (c) Geometry of the irradiation: the tailored Bessel beam (straight green rod) is set to cross the interface between photoresist and glass substrate so as to ensure a perfect adhesion of the polymerized regions after development.

microscope objective (MO), Olympus, 50×, NA = 0.8) and reconstructed into the photoresist layer. The photoresist sample was mounted on a two-axis translation stage, which was prepared by spin-coating the photoresist (Microchem, SU-8) onto a glass substrate at 1000 rpm. The resulting photoresist film thickness was approximately 40 µm, with corresponding soft-baking and hard-baking times of 4 and 5 minutes, respectively.

3. Results and discussion

To achieve our fabrication objective of controlling high-aspect-ratio voxels, a set of beams are employed for demonstration. We use $k_{z0} = 12.1\ \mu m^{-1}$, corresponding to a central spot of ~1.3 µm full width at half maximum, with the preset on-axis intensity plateau length $L_{plateau}$ varied between 15 µm and 25 µm after being demagnified. Figure 2(a) shows the experimental characterization of different beams, the on-axis intensities of these beams are engineered to remain constant over a length $L_{plateau}$ with both parabolic axial profiles on the ascending and falling edges. Here, we fix the position of the falling edges, while axially shifting the ascending edges to change the beam length. We observe, as expected that the axial positions of the falling edges are precisely identical across the different patterns. From one beam to another, only the phasemask is modified.

Now we demonstrate that the fabricated voxel height H_{voxel} can be effectively linearly controllable via the Bessel beam plateau length $L_{plateau}$. Figure 2(b) shows the measured distribution of the normalized on-axis intensity $I(z)/I_{max}$ with the axial position z. Note that we use a common normal maximum intensity $I_{max}^{com} = I_{max}(L_{plateau})$ for tailored Bessel beams with different preset plateau lengths $L_{plateau}$ in accordance with our experiments. Considering the threshold behavior in TPP, we define the axial distance over which the on-axis intensity exceeds a specified virtual threshold $I_{th} = \xi \cdot I_{max}$ as the effective length L_{eff} with ξ representing the normalized intensity threshold relative to the maximum intensity I_{max}. And the evolution of effective length L_{eff} with the plateau length $L_{plateau}$ are presented in Fig. 2(c). For a wide

Optics EXPRESS

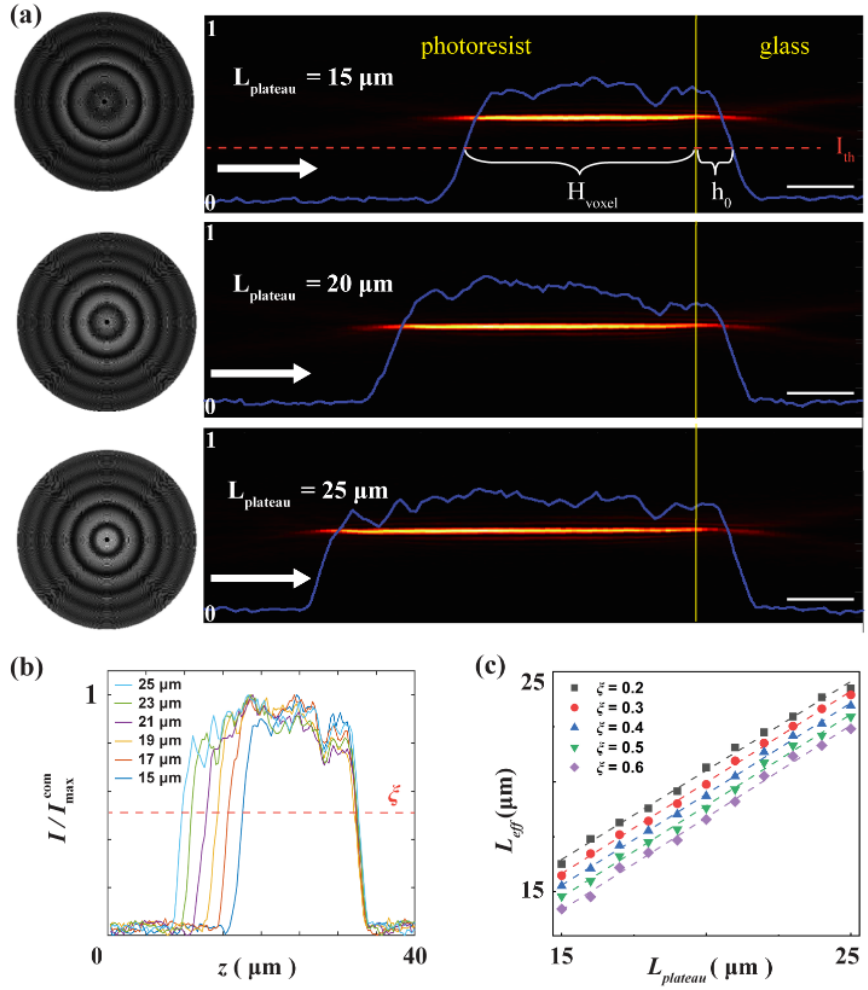

Fig. 2. Controlling the length of Bessel beams via axial intensity tailoring. (a) Normalized axial intensity distribution of tunable-length Bessel beams and the according complex encoded phase mask. The vertical yellow line indicates the schematic interface between the glass substrate and the photoresist layer. All scale bars represent 5 µm. (b) Intensity axial distribution of beams with different lengths: it is apparent that, when the intensity is sufficiently high compared to the TPP threshold, the polymerization length can be linearly controlled. (c) The experimental value of the effective length L_{eff} as a function of the programmed $L_{plateau}$ for different normalized intensity threshold ξ. The dashed lines are obtained by linear fitting of the datasets.

range $0.2 \leq \xi \leq 0.6$, the linear fitting results evidently demonstrate a linear relationship between L_{eff} and the preset $L_{plateau}$: $L_{eff} = L_{plateau} \cdot \alpha + \beta$, where the constant α represents the scaling difference between the actual optical system and an ideal one. β is a factor that only depends on I_{th}. It corresponds to the effective length contribution from the beam intensity profile's rising and trailing edges. Further, taking the beam elongation caused by refraction at the air-photoresist interface and other practical processing influences into account and assuming a factor $\gamma_{(\alpha, \quad I_{\max})}$ representing the linear contribution of these effects to the voxel height under given exposure parameters, the relationship between the voxel height H_{voxel} and the preset beam length $L_{plateau}$

Optics EXPRESS

can be expressed as:

$$H_{voxel} + h_0 = \gamma_{(\alpha,\ I_{max})} \cdot L_{plateau} + \beta \tag{3}$$

Here, h_0 is the penetration depth of the effective length L_{eff} into the substrate. In practical two-photon polymerization processes, the exact value of the intensity threshold may not be precisely measured. However, by appropriately selecting the exposure intensity, we can achieve accurate control over the height variation ΔH_{voxel} between the voxels produced by beams with length variation $\Delta L_{plateau}$ as:

$$\Delta H_{voxel} = \gamma_{(\alpha,\ I_{max})} \cdot \Delta L_{plateau} \tag{4}$$

We stress that, due to the identical on-axis maximum intensity and endpoint of the plateau profiles shared by the tailored Bessel beams, tunable voxel height can be realized simply by switching CGHs without axially shifting the sample or adjusting the input power. Even if our current SLM has a normally slow 17msec refresh time, our scheme still offers at least one order of magnitude faster efficiency than the point-by-point 3D LDW or the beam-shifting strategy due to the mechanical latency and unstability in motion. Thanks to the fixed fabrication time, our strategy offers higher enhancement for longer voxels in comparison with mechanical motion strategies. Employment of a fast spatial light modulator may further enhance the throughput. Via this processing strategy, an array of 32 HAR voxels with various heights is fabricated in 5 s, with aspect ratio (AR) ranging from approximately 7:1 to 15:1.

Figure 3(a) presents a 30° scanning electron microscope (SEM) image of micropillars with linearly graded heights from 8 µm to 16 µm (AR, 7:1 ∼ 15:1), produced in a single exposure each using beams with $L_{plateau}$ ranging from 15 µm to 20 µm. The exposure time was fixed at 0.1 s and the power is set to be 0.012 mW (0.12 nJ) at the sample, with the beam of $L_{plateau}$ = 25 µm serving as the power reference, the factor $\gamma_{(\alpha,\ I_{max})}$ was calibrated to be 1.32 under these exposure parameters. As shown in Figs. 3(b) and 3(c), the fabricated voxels exhibit needle-like morphologies, matching the intensity distribution of the light field above the TPP threshold. Due to the gradual rise of light intensity, the part exposed by light field where the intensity near the threshold region forms the tip, while the part exposed by the intensity plateau forms the uniform cylindrical body.

To evaluate the reproducibility of digital height tuning, we fabricated an array of 10×10 micropillars with 10 different heights using beam with $L_{plateau}$ varying from 15 µm to 25 µm. As illustrated in Fig. 3(d), the measured height agrees well with the height variations predicted by Eq. (4), with a maximum deviation of less than 4%, confirming the validity of our holographic voxel height control method. We also examined the variation in lateral dimensions of the voxels using another array of 96 micropillars with linearly varying voxel heights. As presented in Fig. 3(e), the lateral size remains constant at about 1.3 µm with < 5% variation along with the voxel height changing from 18 µm to 31 µm (AR, 14:1 ∼ 24:1). This feature benefits from the fact that beams with different $L_{plateau}$ share the same maximum on-axis intensity, ensuring that the variations of voxel height do not affect its lateral dimensions. We note that the voxels' ARs stay below 30:1 due to the limit of current setup. But voxels with much higher aspect ratios can be expected as the demonstrated tailored Bessel beams presenting a scaled AR ∼200:1 in our previous work [30]. Besides, non-ideal incident Gaussian beam also results in tiny bending edges of the on-axis intensity plateau [Fig. 2(a)] and asymmetric intensity side lobes [Fig. 4(a)] with similar local peak intensity (∼18% of global peak intensity). Therefore, the exposed power should be carefully calibrated to maintain the local peak intensities below the TPP threshold to achieve high-quality smooth and straight HAR voxels as shown in Fig. 4(b) and (c). Otherwise, bending spindle-like HAR voxels as shown in Fig. 4(d) and (e) would be generated in the over-exposure case, which are induced by the asymmetric intensity side-lobes and bending edges in combination with the accompanying asymmetric mechanical stress. Consequently, voxels generated by our

Optics EXPRESS

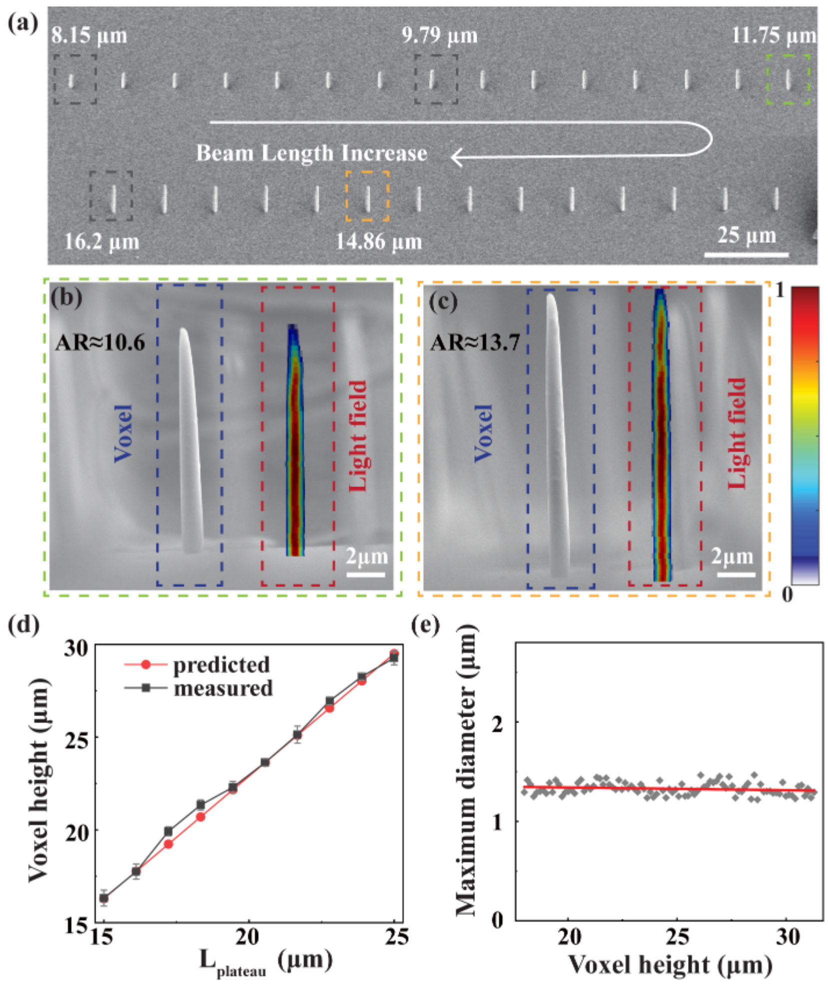

Fig. 3. (a) 30° SEM image of micropillars array with graded height. Close-up view SEM image of single voxels of height, (b) 11.75 µm (AR ~10:1) and (c) 14.86 µm (AR ~13:1) and corresponding light intensity above polymerization threshold. (d) Variation of voxel height with the preset exposure beam length. (e) Variation of voxel maximum lateral diameter with different voxel height.

method allow for simpler voxel configuration design when being assembled into more complex microstructures.

To further demonstrate the potential of this voxel-generation approach for two-photon microfabrication, we produced height-tunable hollow microtubes of different shapes (Fig. 5). Microtubes with high aspect ratios can be rapidly fabricated. By scanning along a circular trajectory, we fabricated the circular microtube array with a diameter of 10 µm and wall thickness of 1.3 µm. The height ranging from 15 µm to 30 µm. To achieve the best surface quality, the spacing between adjacent voxel was set to 200 nm in combination with well selected exposure parameter. As shown in Fig. 5(b), the fabricated microtube heights match well with the theoretical results, confirming the feasibility of our scheme for rapid fabrication of HAR voxel-based microstructures. Furthermore, by employing different transverse scanning patterns, pentagonal and hexagonal microtubes with adjustable heights were also produced.

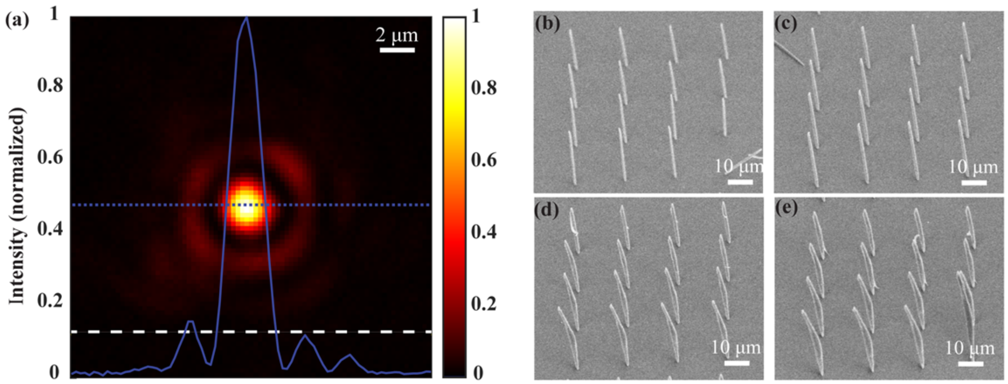

Fig. 4. Impact of sidelobes: (a) a typical intensity profile of the Bessel beam with asymmetric sidelobes, the blue solid line represents the radial profile along the blue dotted line and the white dashed line indicates the relative TPP threshold in the over-exposure case. HAR voxel fabricated: (b) and (c), in proper exposure case; (d) and (e), in over-exposure case.

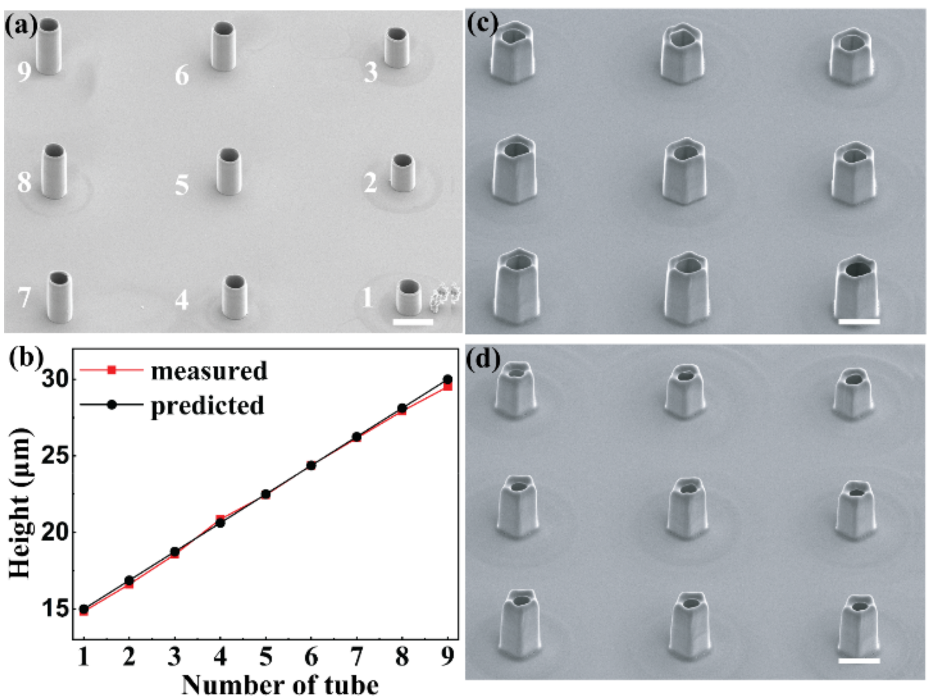

Fig. 5. (a) SEM images of microtubes with graded height. (b) The predicted and measured tube height of different microtubes. SEM images of (c) hexagonal and (d) pentagonal microstructures with graded height. All scale bars represent 20 µm. Ripples on the sample substrates presented in (a), (c) and (d) are residual developer in the unoptimized post-processing procedure. An additional step of rinsing with acetone can totally clean these features.

4. Conclusion

In summary, we have demonstrated a method for fabricating height-tunable high-aspect-ratio voxels using tailored Bessel beams. By tailoring the on-axis intensity profile via a phase-only spatial light modulator (SLM), needle-like voxels with precisely adjustable heights are fabricated in a one-step single exposure, without mechanical axial shift or laser power tuning. The feasibility of the technique is validated through fabricating arrays of microneedle-like voxels and diverse microtubes with graded heights, such as circular microtubes and polygonal arrays. Our method significantly improves writing efficiency compared to conventional point-by-point 3D-LDW strategy. We believe that higher throughput can be achieved by further combined with high-speed spatial light modulators or the multi-foci parallel process in rapid fabrication of functional micro-optical, micro-mechanical and biomedical devices.

Funding. National Natural Science Foundation of China (62275191, 62227821); Tianjin Science and Technology Project (25ZXZSSS00420).

Disclosures. The authors declare no conflicts of interest.

Data availability. Data underlying the results presented in this paper are not publicly available at this time but may be obtained from the authors upon reasonable request.

References

1. Z. Faraji Rad, P. D. Prewett, and G. J. Davies, "High-resolution two-photon polymerization: the most versatile technique for the fabrication of microneedle arrays," Microsyst. Nanoeng. **7**(1), 71–87 (2021).
2. H. Wang, W. Zhang, D. Ladika, *et al.*, "Two-photon polymerization lithography for optics and photonics: fundamentals, materials, technologies, and applications," Adv. Funct. Mater. **33**(39), 2214211 (2023).
3. H.-C. Luo, Y.-Y. Zhao, X.-Y. Zhao, *et al.*, "Grayscale two-photon 3D printed gradient-refractive-index metamaterial lens for dual-band mid-infrared imaging," APL Photonics **9**(5), 051303 (2024).
4. G. Gonzalez, I. Roppolo, C. F. Pirri, *et al.*, "Current and emerging trends in polymeric 3D printed microfluidic devices," Addit. Manuf. **55**, 102867 (2022).
5. A. Balena, M. Bianco, F. Pisanello, *et al.*, "Recent advances on high-speed and holographic two-photon direct laser writing," Adv. Funct. Mater. **33**(39), 2211773 (2023).
6. Q. Geng, D. Wang, P. Chen, *et al.*, "Ultrafast multi-focus 3-D nano-fabrication based on two-photon polymerization," Nat. Commun. **10**(1), 2179 (2019).
7. G. Vizsnyiczai, L. Kelemen, and P. Ormos, "Holographic multi-focus 3D two-photon polymerization with real-time calculated holograms," Opt. Express **22**(20), 24217–24223 (2014).
8. L. Zhang, C. Wang, C. Zhang, *et al.*, "High-throughput two-photon 3D printing enabled by holographic multi-foci high-speed scanning," Nano Lett. **24**(8), 2671–2679 (2024).
9. C. Wang, Z. Ye, C. Zhang, *et al.*, "3D holographic volumetric multi-foci array for two-photon lithography," Laser Photonics Rev. **20**(6), e01811 (2026).
10. S. Gu, C. Mao, A. Guell Izard, *et al.*, "3D nanolithography with metalens arrays and spatially adaptive illumination," Nature **648**(8094), 591–599 (2025).
11. Z.-Y. Hu, Z.-N. Tian, H. Fan, *et al.*, "Long focusing range and self-healing Bessel vortex beam generator," Opt. Lett. **45**(9), 2580–2583 (2020).
12. Y. Li, Y. Zou, Z. Guo, *et al.*, "Constructing arbitrary self-similar Bessel-like beams via transverse-longitudinal mapping," Chin. Opt. Lett. **22**(2), 022601 (2024).
13. M. Manousidaki, D. G. Papazoglou, M. Farsari, *et al.*, "Abruptly autofocusing beams enable advanced multiscale photo-polymerization," Optica **3**(5), 525–530 (2016).
14. S. Wang, X. Xu, X. Jia, *et al.*, "Convex silica microlens arrays processed by a Bessel beam femtosecond laser," Opt. Lett. **50**(13), 4470–4473 (2025).
15. Y. Ma, S. Sun, J. Wang, *et al.*, "Research on microchannel fabrication in UV curable resin using combined beam processing," Sci. Rep. **15**(1), 31296 (2025).
16. Y. Yang, E. Jia, C. Xie, *et al.*, "Single-exposure femtosecond laser direct writing of salvinia-inspired micropatterned functional surface," Opt. Laser Technol. **177**, 111199 (2024).
17. E. Jia, C. Xie, N. Xiao, *et al.*, "Two-photon polymerization of femtosecond high-order Bessel beams with aberration correction," Chin. Opt. Lett. **21**(7), 071203 (2023).
18. L. Yang, A. El-Tamer, U. Hinze, *et al.*, "Two-photon polymerization of cylinder microstructures by femtosecond Bessel beams," Appl. Phys. Lett. **105**(4), 041110 (2014).
19. L. Yang, D. Qian, C. Xin, *et al.*, "Two-photon polymerization of microstructures by a non-diffraction multifoci pattern generated from a superposed Bessel beam," Opt. Lett. **42**(4), 743–746 (2017).
20. D. Pan, S. Liu, J. Li, *et al.*, "Rapid fabrication of 3D chiral microstructures by single exposure of interfered femtosecond vortex beams and capillary-force-assisted self-assembly," Adv. Funct. Mater. **32**(4), 2106917 (2022).

Optics EXPRESS

21. V. Ebrahiminejad, Z. Faraji Rad, P. D. Prewett, *et al.*, "Fabrication and testing of polymer microneedles for transdermal drug delivery," Beilstein J. Nanotechnol. **13**, 629–640 (2022).
22. C. Maibohm, O. F. Silvestre, J. Borme, *et al.*, "Multi-beam two-photon polymerization for fast large area 3D periodic structure fabrication for bioapplications," Sci. Rep. **10**(1), 8740 (2020).
23. E. Jiménez-Díaz, C. Peto-Gutiérrez, M. Hautefeuille, *et al.*, "Two-photon polymerization-based fabrication of high aspect ratio pillars for quantifying pituitary pericytes contractility," J. Micromech. Microeng. **35**(7), 075011 (2025).
24. C. Su, S. Yang, C. Ding, *et al.*, "Parallel 3D projection lithography of massive tunable nanopillars for functional structures," Optica **11**(12), 1725–1732 (2024).
25. G. Chen, H. Teng, J. Chen, *et al.*, "Fabrication of sub-diffraction limit high-aspect-ratio nanostructures via laser direct writing," Chin. Opt. Lett. **23**(3), 033602 (2025).
26. H. Cheng, C. Xia, M. Zhang, *et al.*, "Fabrication of high-aspect-ratio structures using Bessel-beam-activated photopolymerization," Appl. Opt. **58**(13), D91–D97 (2019).
27. D. Pan, B. Xu, S. Liu, *et al.*, "Amplitude-phase optimized long depth of focus femtosecond axilens beam for single-exposure fabrication of high-aspect-ratio microstructures," Opt. Lett. **45**(9), 2584–2587 (2020).
28. D. Pan, S. Liu, S. Ji, *et al.*, "Efficient fabrication of a high-aspect-ratio AFM tip by one-step exposure of a long focal depth holographic femtosecond axilens beam," Opt. Lett. **45**(4), 897–900 (2020).
29. M. Manousidaki, D. G. Papazoglou, M. Farsari, *et al.*, "Long-scale multiphoton polymerization voxel growth investigation using engineered Bessel beams," Opt. Mater. Express **9**(7), 2838–2845 (2019).
30. I. Ouadghiri-Idrissi, R. Giust, L. Froehly, *et al.*, "Arbitrary shaping of on-axis amplitude of femtosecond Bessel beams with a single phase-only spatial light modulator," Opt. Express **24**(11), 11495–11504 (2016).